Korean J. Chem. Eng., **25**(4), 939-946 (2008)

Effect of pulse modulation on particle growth during SiH_4 plasma process

Dong-Joo Kim and Kyo-Seon Kim†

Department of Chemical Engineering, Kangwon National University, Chuncheon, Gangwon-do 200-701, Korea
(*Received 9 November 2007 • accepted 7 January 2008*)

Abstract−The effects of pulse modulation on particle growth by coagulation between particles in a pulsed SiH_4 plasma reactor were analyzed by using a discrete-sectional method. At the start of the plasma discharge, there is high concentration of small-sized particles, and, later, the large-sized particles appear and grow by coagulation between small-sized particles. During plasma-off, the monomer generation stops and the particle concentration decreases with time by the effects of particle coagulation and fluid flow. As the pulse frequency decreases or as the duty ratio increases, the large-sized particles grow faster because more monomer particles are generated during longer plasma-on time. These results show that the pulse modulation, the changes of pulse frequency and duty ratio, can play a key role in suppressing the particle growth in the pulsed plasma process efficiently. This study proves that the pulsed plasma process can be applied to reduce the particle contamination in the plasma process for preparation of high quality thin films.

Key words: Pulse Modulation, Pulsed Plasmas, Particle Coagulation, Particle Size Distribution, Plasma Reactor

INTRODUCTION

Many researchers have studied the plasma process for preparation of high quality thin films and nanoparticles with narrowly dispersed particle size distribution. In the conventional, continuous-wave, plasma process for semiconductor fabrication, the particles in the size of less than submicrons can be generated, and they can induce several serious effects on the performance and quality of microelectronic devices and on the cost of final products. Particle contamination control is quite important in the plasma reactor to prepare high quality thin films for semiconductors. Many researchers have attempted to reach the goal of reducing the particle contamination. For example, a low pressure operation can be a possible method for preparing high quality thin films by reducing the particle contamination, but this method has a disadvantage in the slow deposition rate. According to recent reports, the pulsed plasma process can be a relatively simple method for preparing high quality thin films by reducing the particle contamination at a high deposition rate, compared with the continuous-wave plasma at low pressure operation [1-3].

In the pulsed plasma process, one pulse cycle consists of plasma-on with power supply and plasma-off without power supply, and the periods of plasma-on (t_{on}) and -off (t_{off}) are determined by pulse frequency (f_p) and duty ratio ($D=(t_{on})/(t_{on}+t_{off})\times 100$). During t_{on}, the electrons obtain high energy by the electric field and collide with molecules to form radicals and ions. During t_{off}, all electrons disappear and there is no more generation of radicals and ions by electron collision. The pulse repetition can reduce the concentration of precursors (radicals, or ions) for particle generation and growth in the pulsed plasmas, compared with those in the continuous-wave plasmas [1-7].

There are several experimental studies for analyzing the particle growth in pulsed plasma processes. Watanabe's group found that the deposition of few nm's particles results in a deterioration in the quality of the a-Si:H thin films and showed that the growth of nano-sized particles can be suppressed efficiently in the pulse modulated plasma discharges [3]. Kirimura et al. [7] analyzed the effects of plasma parameters on the particle growth and also on the properties of a-Si:H thin films in pulsed plasma processes, and they synthesized high quality a-Si:H films by the amplitude modulated plasmas. Timmons' group [2,8] synthesized fluorocarbon thin film for integrated circuits by adjusting the duty cycles in the pulsed plasma processes. Itagaki et al. [4] could efficiently reduce the particle contamination in the electron cyclotron resonance plasma process for preparation of high quality a-Si:H thin films by pulse modulation. Bapin and Rudolf von Rohr [9] prepared good quality silicon dioxide films by using microwave plasma-enhanced chemical vapor deposition under the pulse mode. Those studies showed that the pulse modulation can play a key role in reducing the particle contamination in the pulsed plasma process, and the pulsed plasma process can be used to prepare high quality thin films.

A systematical analysis of particle growth in the pulsed plasma process is required to understand the effects of pulse modulations on particle growth in the pulsed plasma reactor, and further to apply the pulsed plasma process commercially to prepare high quality thin films. Not enough theoretical studies on particle growth in the pulsed plasma process have been made. On the other hand, the particle growth and transport in the continuous-wave SiH_4 plasma processes has been analyzed systematically by using numerical methods. Specially, Kim's group analyzed the particle growth by coagulation in the SiH_4 plasma reactor using discrete-sectional method, and showed that the particle size distribution in the continuous-wave plasma processes becomes bimodal and large-sized particles become quite monodisperse [10-12].

The goal of this study was to investigate the effects of pulse modulations such as pulse frequency and duty ratio on particle growth in pulsed SiH_4 plasma process theoretically. We also showed the evolutions of particle size distribution in pulsed plasmas during t_{on} and t_{off} for various conditions.

THEORY

Watanabe's group proposed the ideal plasma reactor of parallel

†To whom correspondence should be addressed.
E-mail: kkyoseon@kangwon.ac.kr

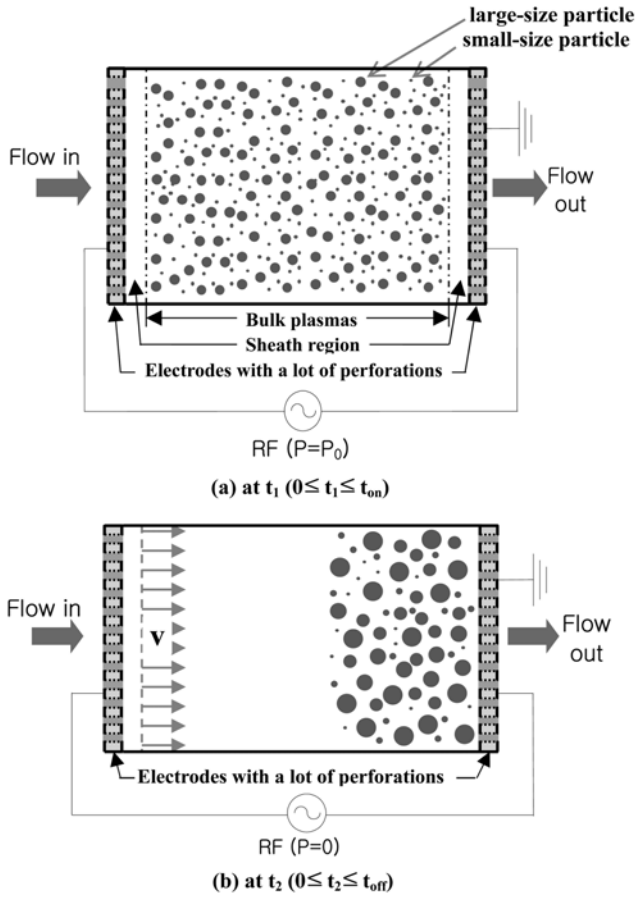

Fig. 1. Model of particle growth in dusty plasmas during (a) plasma-on (t_{on}) and (b) plasma-off (t_{off}).

plate type to analyze the nano-sized particle growth inside the plasma reactor [3]. In their experiments, the upper and lower electrodes are designed to have many perforations so that the gas stream can pass through the electrodes. We considered the plasma reactor proposed by Shiratani et al. [3] as a model reactor to analyze the particle growth, and could expect plug flow for the gas stream inside this plasma reactor and neglect the momentum balance in the model equations.

We analyzed the particle growth by coagulation between particles in a plasma reactor dense with particles, where the particles are dispersed in the bulk plasma region and are believed to grow by coagulation between particles. Fig. 1 shows the model to analyze the particle growth in pulsed plasmas during t_{on} (a) and t_{off} (b). During t_{on}, the plasma reactor was assumed to be a continuously stirred-tank reactor because the negatively charged particles are caught in the bulk plasma region by electrostatic repulsion in the sheath regions [10-12], and, during t_{off}, was assumed to be a plug flow reactor because the plasma sheath regions collapse away and the particles can flow out of the plasma reactor by fluid convection.

The aerosol dynamic equation for particles in plasma reactor includes the terms of fluid flow, particle generation and coagulation in a plasma reactor. This aerosol dynamic equation is a nonlinear, partial integro-differential equation. An appropriate approach should be used to solve this equation to predict the evolution of the particle size distribution within limited computing time. The discrete-sectional model can reduce the computing time and is good for predicting the particle size distribution where the particles grow by coagulation [13-15]. We used volume-conserved discrete-sectional model equations to analyze numerically the particle growth in the pulsed plasma reactor in this study. In the discrete-sectional model, the aerosol size spectrum is divided into two regimes: discrete-size regime (DSR) and sectional-size regime (SSR) [13,16]. The governing equation for volume concentration, q_i, of *i*-mers (*i*=1 to *i*max) in DSR can be expressed as follows [10,12]:

$$\frac{dq_i}{dt}=\frac{S_1}{\rho_p}\delta(v-v_1)+\frac{1}{2}\sum_{j=1}^{i-1}(E_{j,(i-j)}\beta^{*}_{j,(i-j)}q_j q_{(i-j)}) - q_i\sum_{j=1}^{i\,max}(E_{i,j}\beta^{*}_{i,j}q_j)-q_i\sum_{k=1}^{k\,max}(E_{i,k}{}^{4}\overline{\beta}^{D}_{i,k}Q_k)-(F_{pos,i}+F_{neu,i})\frac{q_i}{\tau_{res}}. \quad (1)$$

In Eq. (1), the first term in right hand side (RHS) is the generation rate of q_1 for monomers. The second term in RHS is the generation rate of q_i by coagulation of smaller particles, and the next two terms are the disappearance rates of q_i by coagulation of *i*-mers with DSR and SSR particles, respectively. The final term in RHS is the effect of fluid flow. The governing equation for volume concentration, Q_k, of the *k*th section particles (k=1 to kmax) in SSR can be expressed as follows [10,12]:

$$\frac{dQ_k}{dt}=\frac{1}{2}\sum_{i=1}^{i\,max}\sum_{j=1}^{i\,max}(E_{i,j}{}^{1}\overline{\beta}^{DD}_{i,j,k}q_i q_j)+\sum_{i=1}^{i\,max}\sum_{j=1}^{k-1}(E_{i,j}{}^{1}\overline{\beta}^{D}_{i,j,k}q_i Q_j) +\frac{1}{2}\sum_{i=1}^{k-1}\sum_{j=1}^{k-1}(E_{i,j}{}^{1}\overline{\beta}_{i,j,k}Q_i Q_j)-Q_k\sum_{i=1}^{i\,max}(E_{i,k}{}^{2}\overline{\beta}^{D}_{i,k}q_i)+Q_k\sum_{i=1}^{i\,max}(E_{i,k}{}^{5}\overline{\beta}^{D}_{i,k}q_i) -Q_k\sum_{i=1}^{k-1}(E_{i,k}{}^{2}\overline{\beta}^{D}_{i,k}Q_i)+Q_k\sum_{i=1}^{k-1}(E_{i,k}{}^{5}\overline{\beta}^{D}_{i,k}Q_i)-\frac{1}{2}E_{k,k}{}^{3}\overline{\beta}_k Q_k^2 -Q_k\sum_{i=k+1}^{k\,max}(E_{i,k}{}^{4}\overline{\beta}^{D}_{i,k}Q_i)-(F_{pos,(i\,max+k)}+F_{neu,(i\,max+k)})\frac{Q_k}{\tau_{res}}. \quad (2)$$

In Eq. (2), the first three terms in RHS are the generation rates of Q_k by coagulations between two DSR particles, between one DSR and one smaller SSR particle, and between two smaller SSR particles, respectively. The fourth and fifth terms are the disappearance and generation rates, respectively, of Q_k by coagulations between one DSR and one section-*k* particle. The sixth and seventh terms are the disappearance and generation rates, respectively, of Q_k by coagulations between one smaller SSR and one section-*k* particle. The eighth and ninth terms are the loss rates, respectively, of Q_k by coagulations between two section-*k* particles and between one section-k and one larger section particle. The final term accounts for the loss of Q_k by fluid flow.

During t_{on}, the particles can be charged positively or negatively or in neutral state by Matsoukas and Russell [17], and we can calculate the fractions of particles charged positively or negatively or in neutral state from the particle charge distribution function and use them to obtain the collision frequencies between particles. The particles of opposite charges will collide with each other very fast and the neutral particles can collide with all particles, but the particles of same charges cannot collide together. The enhancement factor of collision frequency function, $E_{i,j}$, taking into account the particle charge distribution of colliding particles in Eqs. (1), (2) can be calculated as follows [10,12]:

$$E_{i,j}=[F_{i,neu}F_{j,neu}+F_{i,neu}F_{j,neg}+F_{i,neu}F_{j,pos}+F_{i,neg}F_{j,neu} +F_{i,neg}F_{j,pos}(1-\Gamma_{i,j})+F_{i,pos}F_{j,neu}+F_{i,pos}F_{j,neg}(1-\Gamma_{i,j})], \quad (3)$$

$$\Gamma_{i,j} = \frac{\overline{z}_{i,(neg\ or\ pos)}\overline{z}_{j,(pos\ or\ neg)}e^2}{\pi\varepsilon_0 m_R v_R^2 (d_i + d_j)}. \quad (4)$$

$(1-\Gamma_{i,j})$ in Eq. (3) is the enhancement factor of collision frequency function induced by the Coulomb force between the oppositely charged particles colliding together. The positively charged or neutral particles go out of the reactor with fluid flow, but the negatively charged particles are caught inside the plasma reactor by electrostatic repulsion [10-12]. The monomers are assumed to be generated only during t_{on}.

During t_{off}, the monomers are not generated anymore and the concentrations of electrons and positive ions become zero quickly in plasma reactor. All particles lose their charges to become neutral and they can go out of the reactor by fluid convection. We used the collision frequency function between neutral particles to calculate particle coagulation rate during t_{off}. In pulsed plasmas, the changes of electron and ion concentrations occur within 10's μsec just after plasma-on or -off [18-21]. The pulse frequency ranges from 1 Hz to 1,000 Hz in this study, corresponding to the t_{on} or t_{off} from 1 s to 5×10^{-4} s (500 μsec) at the duty ratio of 50%, and the t_{on} or t_{off} is much longer than 10's μsec, and we assumed that the changes of electron and ion concentrations just after t_{on} or t_{off} do not significantly affect the particle charging during t_{on} or t_{off}.

The governing equations for volume concentrations of particles in DSR and SSR were solved numerically by the ODE solver, the VODPK subroutine, to predict the particle size distribution in the plasma reactor during t_{on} and t_{off}. During t_{on}, the electron concentration changes with time as the particle concentration and size change in plasma reactor. We calculated the electron concentration in every time step of integration by solving the electroneutrality condition and used it to predict the particle charge distributions. During t_{off}, the plasma reactor is divided into two regions (regions where particles exist and do not exist) based on the assumption of plug flow reactor (Figs. 1(b)). In the region where particles exist, the particles will grow by coagulation between neutral particles. The particle concentrations during t_{off} are calculated by averaging for the whole reactor volume by multiplying (reactor volume with particles)/(total reactor volume).

RESULTS AND DISCUSSION

The pulse frequency and duty ratio ranged from 0.5 to 1000 Hz and from 20 to 80%, respectively, to investigate the effects of those variables on particle size distribution in pulsed SiH_4 plasmas during t_{on} and t_{off}. The standard conditions for S_1, d_1, τ_{res}, f_p and D were 4.23×10^{-7} g/cm^{3}s, 10 nm, 0.5 s, 1 Hz and 50%, respectively. The charge distributions of particles during t_{on} are expressed in terms of electron and positive ion concentrations, and ion and electron temperatures which were assumed to be 6.0×10^{10} cm^{-3}, 5.0×10^{9} cm^{-3}, 300 K and 2 eV, respectively, in this study. The positive and negative ion concentrations in the plasma reactor reach the steady state very quickly in comparison with t_{on}. To calculate the electron concentration to satisfy the electroneutrality condition in the plasmas, we assumed that those concentrations are constant during plasma-on [10].

Fig. 2 shows the change of particle size distribution with time ($0<t\leq1$ s) for a pulse frequency of 1 Hz and duty ratio of 50%. The

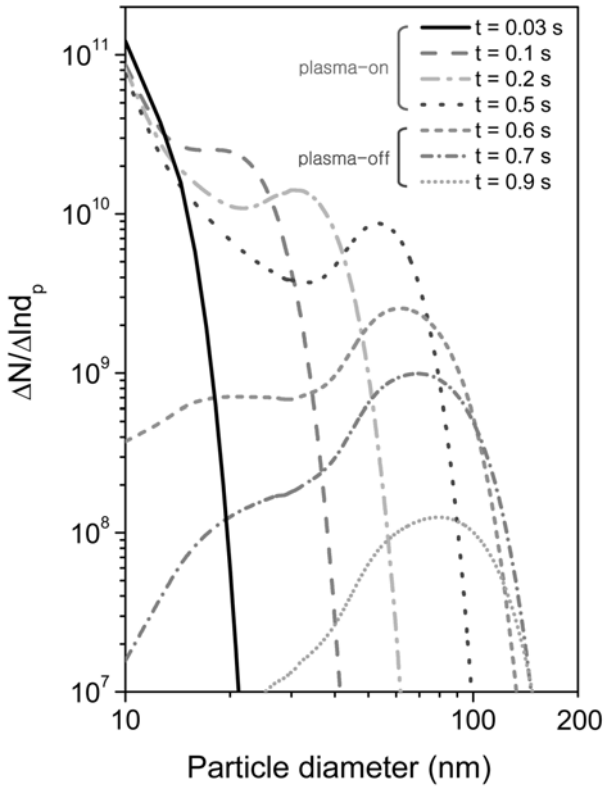

Fig. 2. Particle size distributions for various times (d_1=10 nm, f_p= 1 Hz, τ_{res}=0.5 s, D=50%).

plasma is on for $0<t\leq0.5$ s and is off for $0.5<t\leq1$ s. In the beginning of plasma-on (at $0<t\leq0.03$ s), the monomer ($d_1\approx10$ nm) concentration becomes high because of fast monomer generation rate, and the concentration of small-size particles ($10\text{ nm}<d_p\leq20$ nm) increases quickly because the small-sized particles are generated fast by coagulation between smaller particles. At t=0.1 s, the large-sized particles appear by coagulation between small-sized particles and grow for $0.1\leq t\leq0.5$ s and, at t=0.5 s, the particles inside plasma reactor becomes bimodal of small-sized and large-sized particles. During t_{off} ($0.5<t\leq1$ s), the particles in all size regimes are in neutral state and they will go out of the reactor by fluid convection. The small-sized particle concentration decreases quickly because the monomer generation stops and the small-sized particles disappear by fast coagulation with other particles. The large-sized particle concentration decreases slowly because the large-sized particles are still generated by coagulation with small-sized particles during t_{off}. At t=0.9 s, the particle size distribution becomes monodisperse with large-sized particles. The large-sized particles during t_{on} grow more quickly by the faster coagulation with small-sized particles than during t_{off}, because the small-sized particle concentration during t_{on} is higher than during t_{off}. At the end of t_{off}, there is no particle remaining inside the reactor because all particles flow out of the reactor (t_{off} of 0.5 s is equal to τ_{res} of 0.5 s) by fluid convection and the particle size distribution in the next pulse cycle is not affected by that in the previous pulse cycle.

Fig. 3 presents the evolution of particle size distribution during t_{on} ($2.5<t\leq2.75$ s) and t_{off} ($2.75<t\leq3.0$ s) for the pulse frequency of 2 Hz and duty ratio of 50%. The t_{off} here is shorter than τ_{res} and the

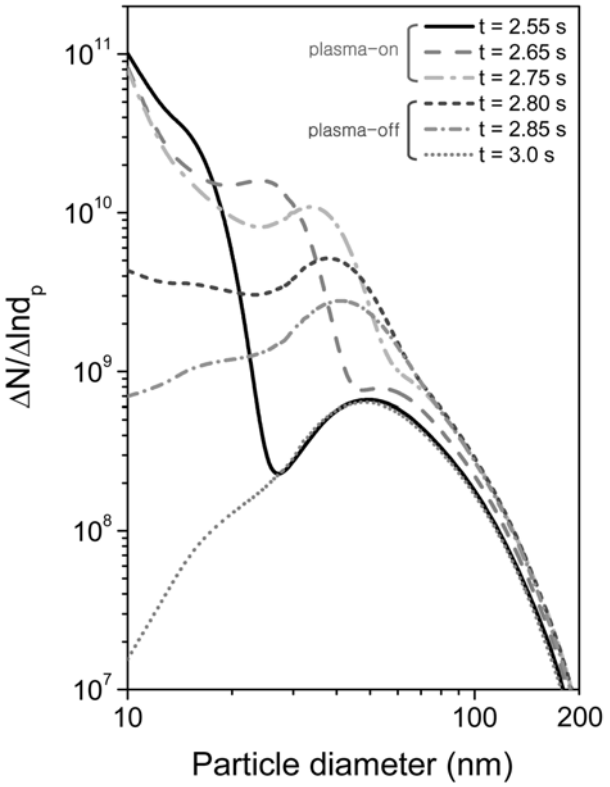

Fig. 3. Particle size distributions for various times (d_1=10 nm, f_p= 2 Hz, τ_{res}=0.5 s, D=50%).

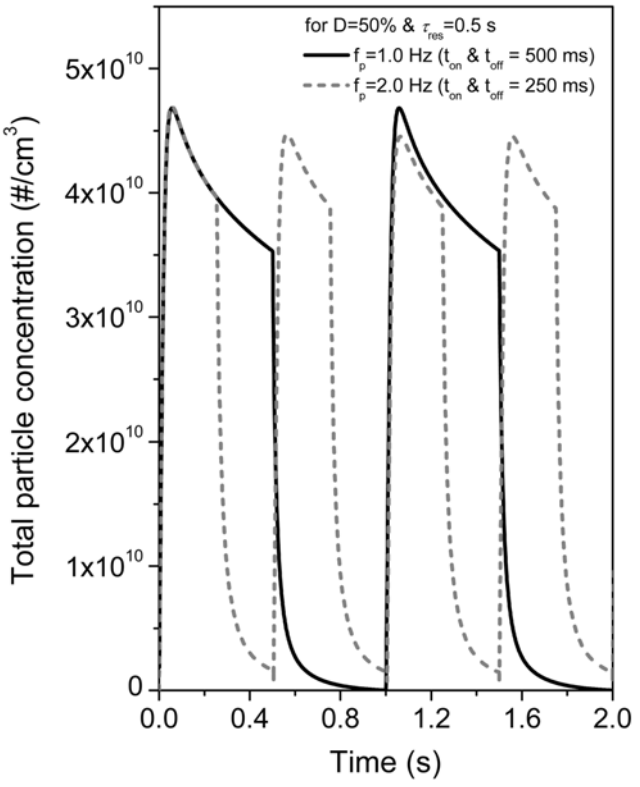

Fig. 4. Total particle concentrations averaged over the plasma reactor for various pulse frequencies (d_1=10 nm, τ_{res}=0.5 s, D= 50%).

particles generated in the previous cycle are not swept out of the reactor completely during t_{off}. The particle size distribution in the next cycle is affected by that in the previous cycle. At t=2.55 s, the particles in the plasmas are classified into two groups: the small-sized particles ($10 \le d_p < 25$ nm) appeared quickly by the fast monomer generation and the large-sized particles ($25 \le d_p < 200$ nm) are left over from the previous pulse cycle. At t=2.65 s, the medium-sized particles ($15 \le d_p \le 45$ nm) appear and grow by fast coagulation between small-sized particles of high concentration ($2.65 \le t \le 2.75$ s) and, at t=2.75 s, the particle size distribution becomes trimodal of small-sized, medium-sized and the large-sized particles. During t_{off} ($2.75 < t \le 3.0$ s), the particle concentration decreases with time because of particle loss by particle coagulation and fluid convection without particle generation. The concentration of small-sized particles decreases more quickly than that of large-sized particles, because the generation of monomers and small-sized particles stops and some large-sized particles continue to be generated by coagulation between smaller particles. In Fig. 3, the t_{off} is too short for all particles to flow out of the plasma reactor by fluid convection and the particles are still remaining inside the plasma reactor at the end of plasma-off (t=3.0 s). The particle size distribution at t=3.0 s becomes the initial condition to calculate the particle size distribution in the next cycle and we come to have the large-sized particles from the beginning of plasma-on in the next cycle.

Figs. 4 and 5 show the changes of total particle concentration and mean particle diameter averaged over the plasma reactor for two different pulse frequencies of 1 and 2 Hz, respectively. As shown in Figs. 2 and 3, the concentration of small-sized particles changes quickly with time during one cycle and the evolutions of total particle concentration and mean particle diameter are strongly affected by the amount of small-sized particles. In Fig. 4, at the start of plasma-on, the particle concentration increases quickly, because the monomer particles are generated fast, and the total particle concentration reaches maximum and, later, decreases with time until the end of t_{on}, because the particle coagulation rate at high concentration is faster than new particle generation rate. During t_{off}, the monomer particles are not generated any more and total particle concentration decreases quickly by particle coagulation and fluid convection, becoming zero when all the particles are carried away from the plasma reactor by fluid convection. In Fig. 5, the mean particle diameter increases until the end of t_{on}, because the particles continue to grow by coagulation with small-sized particles during t_{on}. During t_{off}, new small particles are not generated any more and the mean particle diameter increases fast by particle coagulation and becomes zero when there is no particle remaining in the plasma reactor. As the pulse frequency for a given duty ratio decreases, t_{on} and t_{off} increase, new particle generation takes place longer, the residence time of particles inside the reactor increases, and the maximum mean particle diameter becomes larger by the longer coagulation time (Fig. 5). In Figs. 4 and 5, for a pulse frequency of 1 Hz ($t_{off}=\tau_{res}$), total particle concentration becomes zero at the end of t_{off}, because all the particles are carried out by fluid convection, and the transient behaviors of total particle concentration and mean particle diameter will be same for every pulse cycle. For a pulse frequency of 2 Hz where t_{off} (=0.25 s) is shorter than τ_{res} (=0.5 s), total particle con-

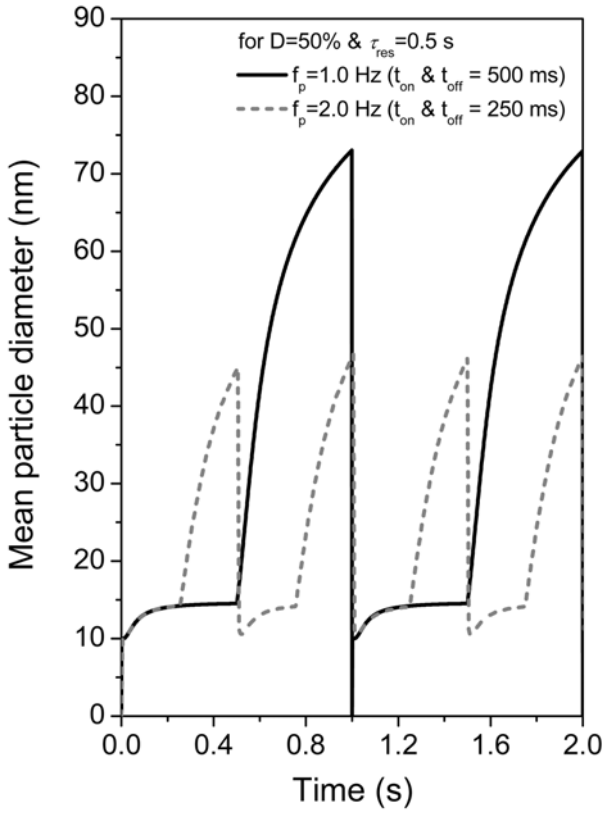

Fig. 5. Mean particle diameters averaged over the plasma reactor for various pulse frequencies (d_1=10 nm, τ_{res}=0.5 s, D=50%).

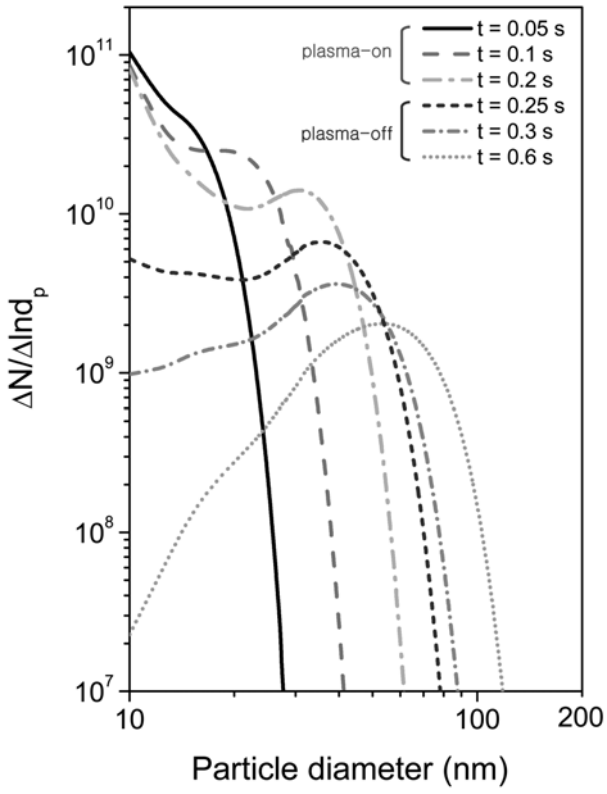

Fig. 6. Particle size distributions for various times (d_1=10 nm, f_p= 1 Hz, τ_{res}=0.5 s, D=20%).

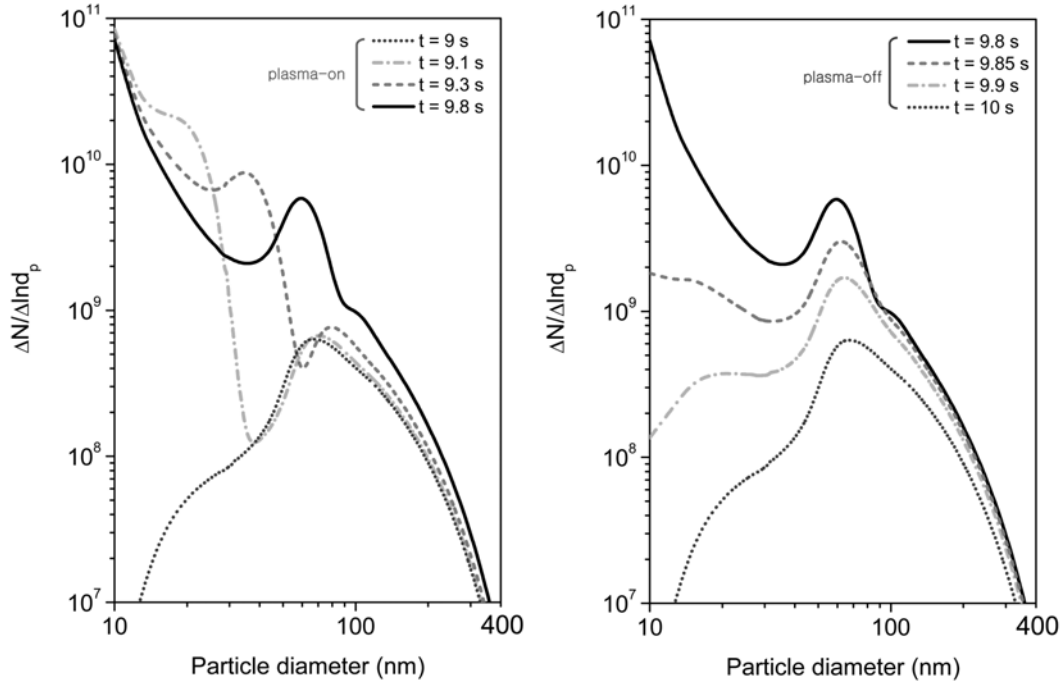

Fig. 7. Particle size distributions for various times during (a) plasma-on and (b) plasma-off (d_1=10 nm, f_p=1 Hz, τ_{res}=0.5 s, D=80%).

centration at the end of t_{off} is not zero, because some particles still remain inside the plasma reactor at the end of t_{off}. The particles generated in the previous pulse cycle will affect the transient behaviors of total particle concentration and mean particle diameter in the next pulse cycle.

The evolutions of particle size distributions during t_{on} and t_{off} for

two duty ratios of 20 and 80% are shown in Figs. 6 and 7, respectively. During t_{on}, the large-sized particles grow by coagulation with the small-sized particles of high concentration and, during t_{off}, the small-sized particle concentration decreases quickly while the large-size particle concentration decreases slowly, because some large-sized particles continue to be generated by coagulation between smaller particles. In Fig. 6, at the end of t_{on} (t=0.2 s), the particle size distribution becomes bimodal of small-sized and large-sized particles and, at t=0.6 s, becomes monodisperse with large-sized particles. Fig. 7(a) shows the particle size distributions during t_{on} (9.0<t≤9.8 s). The particles generated in the previous cycle are not swept out completely during t_{off} because the t_{off} is shorter than τ_{res} and the particle size distribution at t=9.0 s is the result from the previous pulse cycle. At t=9.1 s, we come to have three modes of particle size distribution: the small-sized particles ($10 \le d_p < 15$ nm) appeared quickly by the fast monomer generation, the medium-sized particles ($15 \le d_p < 35$ nm) appeared by fast coagulation between small-sized particles of high concentration, and the large-sized particles ($35 \le d_p < 400$ nm) are left over from the previous pulse cycle. The medium-sized and large-sized particles continue to grow by coagulation with small-sized particles during t_{on}. At the end of t_{on}, the particle size distribution is still trimodal of small-sized, medium-sized and large-sized particles. During t_{off} (9.8<t≤10 s) (Fig. 7(b)), the concentration of small-sized particles decreases more quickly than that of large-sized particles, because the large-sized particles continue to be generated by coagulation between smaller particles with no generation of small-sized particles, and, at t=10 s, some particles are still remained inside the reactor.

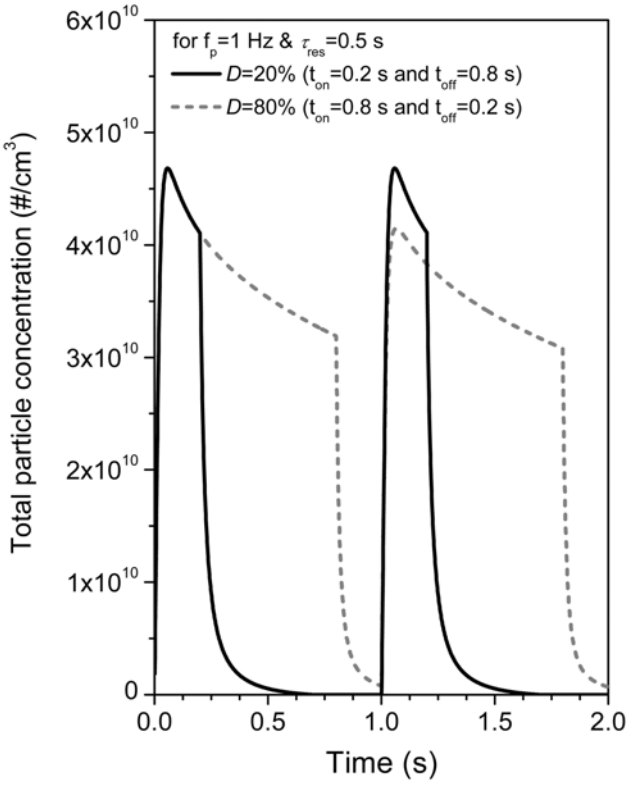

Fig. 8. Total particle concentrations averaged over the plasma reactor for various duty ratios (d_1=10 nm, f_p=1 Hz, τ_{res}=0.5 s).

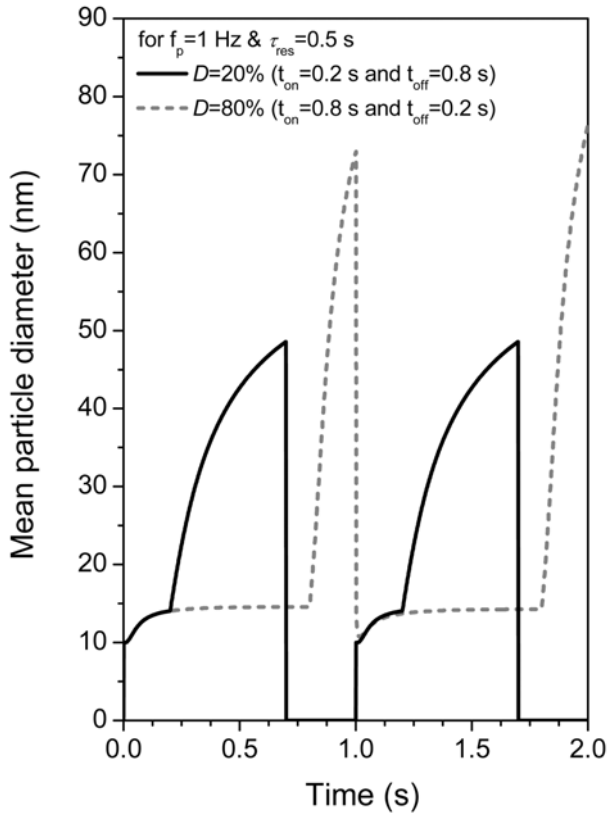

Fig. 9. Mean particle diameters averaged over the plasma reactor for various duty ratios (d_1=10 nm, f_p=1 Hz, τ_{res}=0.5 s).

Figs. 8 and 9 show the changes of total particle concentration and mean particle diameter averaged over the plasma reactor for two different duty ratios of 20 and 80%, respectively. In Fig. 8, during t_{on}, the total particle concentration increases quickly and reaches maximum and, later, decreases with time until the end of t_{on} by the fast particle coagulation. After the plasma-off, the total particle concentration decreases quickly by particle coagulation and also by fluid convection until the end of t_{off}. In Fig. 9, during t_{on}, the mean particle diameter increases slowly because new monomers are generated and the particles continue to grow by particle coagulation until the end of t_{on}. During t_{off}, the mean particle diameter increases quickly by particle coagulation without monomer generation until there are some particles in the plasma reactor. In Fig. 8, for a duty ratio of 20% ($t_{off} > \tau_{res}$), total particle concentration becomes zero during t_{off}, because all the particles are carried out by fluid convection. For the duty ratio of 80% where t_{off} (=0.2 s) is shorter than τ_{res} (=0.8 s), total particle concentration at the end of plasma-off is not zero, because some particles still remain inside the plasma reactor. In Fig. 9, as the duty ratio increases from 20% to 80%, the maximum mean particle diameter becomes larger because the t_{on} for new particle generation and particle coagulation increases. For a duty ratio of 80%, the maximum total particle concentration in the second pulse cycle is lower than that in the first cycle, and the maximum mean particle diameter in the second cycle is larger than that in the first cycle, because the large-size particles are not swept way completely in the previous cycle; they continue to grow by coagulation with small-sized particles generated in the next pulse cycle.

In continuous-wave plasmas, the particle size distribution in the plasma reactor becomes clearly bimodal with small-sized and large-sized particles and the mode of large-sized particles becomes quite narrow [10-12]. In pulsed plasmas, the particle size distribution changes with time during the cycle, and there is no clear discrepancy in the particle size distribution between two size modes, compared with that in continuous-wave plasmas. The large-sized particles in pulsed plasmas become smaller than those in continuous-wave plasmas because pulse modulation prevents the growth of large-sized particles in pulsed plasmas. The results from Figs. 2 to 9 show that the particle concentration and size can be reduced with the increase in pulse frequency or with the decrease in duty ratio, and also that the pulse frequency and duty ratio can be key parameters to reduce the particle contamination in pulsed plasma process.

Fig. 10 shows the mean particle diameters in continuous-wave and pulsed plasmas for various pulse frequencies, and also shows the comparisons by experiments [3] and by numerical method in this study for the same process conditions. In Shiratani et al.'s experiments, after plasma-off, the particles are redistributed inside the plasma reactor by particle diffusion, and the diameter of those particles is determined from their diffusivity measured by photo-counting laser-light-scattering method. The predicted mean particle diameter was obtained from the particle size distribution at $0.5t_{off}$ after plasma-off by averaging the particles in all size regimes. In pulsed plasmas, the mean particle diameter becomes smaller than that in continuous-wave plasmas because the amount of monomer particles generated during t_{on} is smaller than that in continuous-wave plasmas, and also the particles flow out of the reactor during t_{off}. As the pulse frequency in pulsed plasmas decreases, new monomer generation and coagulation for particle growth take longer time during t_{on} in each pulse cycle and the mean particle diameter increases. The model results were in good agreement with the published experimental data [3]. Both results by experiments and numerical method prove that the particle generation and growth in SiH_4 PCVD process can be suppressed by the pulsed plasma method, which is important for preparing high quality thin films in the SiH_4 PCVD process.

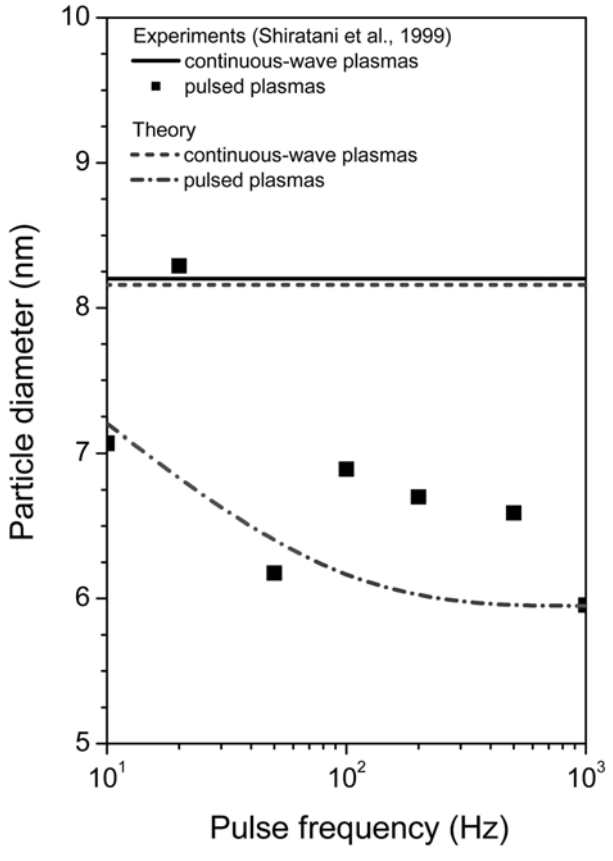

Fig. 10. Mean particle diameters in continuous-wave and pulsed plasmas for various pulse frequencies by experiments [3] and by numerical method for the same process conditions.

CONCLUSIONS

We analyzed the particle growth in pulsed SiH_4 plasmas during plasma-on and -off numerically, changing the pulse frequency and duty ratio, which are believed to play a key role in the evolution of particle size distribution in pulsed plasma process. During plasma-on, the plasma reactor was assumed to be a continuously stirred-tank reactor, but during plasma-off, was assumed to be a plug flow reactor. Just after plasma-on, we have a high concentration of small-sized particles and, later, large-sized particles appear and grow by coagulation between small-sized particles. During plasma-off, the monomer generation stops and the particle concentration decreases with time by the effects of particle coagulation and fluid flow. For t_{off} longer than residence time, the particle size distribution in pulsed plasmas becomes bimodal with small-sized and large-sized particles in the end of t_{on}, while for t_{off} shorter than residence time, becomes trimodal with small-sized, medium-sized and large-sized particles in the middle of t_{on}, because the large-sized particles formed in the previous cycle still remain inside the plasma reactor until the end of t_{off} and they affect the particle size distribution in the next cycle. As the pulse frequency decreases or as the duty ratio increases, more monomer particles are generated during longer plasma-on time and the large-sized particles become bigger at the end of t_{on}. This study shows that the pulse plasma process can be used to suppress the particle growth in SiH_4 plasma process and can be a good method for preparing high quality thin films by reducing the particle contamination.

ACKNOWLEDGMENTS

This work is financially supported by the Ministry of Education and Human Resources Development (MOE) and the Ministry of Commerce, Industry and Energy (MOCIE) through the fostering project of the Industrial-Academic Cooperation Centered University.

NOMENCLATURE

d_1 : monomer diameter [nm]
d_l : particle diameter in the lth discrete size regime or sectional size regime [cm]
d_p : particle diameter [nm]
D : duty ratio [%]
e : elementary charge of electron [C]
$E_{i,j}$: enhancement factor of collision frequency function

f_p : pulse frequency [Hz]
$F_{l,neg}$, $F_{l,neu}$, $F_{l,pos}$: fractions of particles which are charged negatively, neutral, or charged positively in *l*th discrete size regime or sectional size regime
m_R : reduced mass between the moving particles
q_i : volume concentration variable for i-mers in the discrete size regime
Q_k : volume concentration variable for section k particles
S_1 : mass generation rate of monomers [g/cm^{3}s]
t : time [s]
t_{on} and t_{off} : times for plasma-on and -off [s]
v : particle volume variable [cm^3]
v_1 : monomer volume [cm^3]
v_k : particle volume upper boundary of sectional k [cm^3]
v_{k-1} : particle volume lower boundary of sectional k [cm^3]
v_R : relative velocity between the moving particles
z : particle charges [e]
$\bar{z}_l$: average charges of particle in *l*th discrete size regime or sectional size regime [e/particle]

Greek Letters

$\beta^*_{i,j}$: general property coagulation coefficient ($\beta_{i,j}/(jv_1)$) [14]
$\bar{\beta}^D_{i,k}$: collision integral for coagulations of section k particles and i-mers in discrete size regime [14]
$\bar{\beta}^{DD}_{i,j,k}$: collision integral for coagulations of two discrete size regime particles [14]
ε_0 : permittivity of free space=8.854×10^{-21} [C^2/dyn·cm^2]
ρ_p : particle density [g/cm^3]
τ_{res} : residence time [s]

Subscripts

0 : initial
e : electron
l : *l*th discrete size regime or sectional size regime
+ : positive ion
− : negative ion

REFERENCES

1. A. Madan and S. Morrison, *Solar Energy Mater. Solar Cells*, **55**, 127 (1998).
2. C. R. Savage, R. B. Timmons and J. W. Lin, in *Structure property relations in polymers*, ACS advances in Chem. Series, edited by M. W. Urban and C. D. Craver, 236, 745 (1993).
3. M. Shiratani, T. Fukuzawa and Y. Watanabe, *Jpn. J. Appl. Phys*., **38**, 4542 (1999).
4. N. Itagaki, A. Fukuda, T. Yoshizawa, M. Shindo, Y. Ueda and Y. Kawai, *Surf. Coat. Technol*., **131**, 54 (2000).
5. D.-J. Kim and K.-S. Kim, *Ind. Eng. Chem. Res*., **44**, 7907 (2005).
6. K.-S. Kim, D.-J. Kim and Q.-Q. Zhao, *Chem. Eng. Sci*., **61,** 3278 (2006).
7. H. Kirimura, H. Maeda, H. Murakami, T. Nakahigashi, S. Ohtani, T. Tabata, T. Hayashi, M. Kobayashi, Y. Mitsuda, N. Nakamura, H. Kuwahara and A. Doi, *Jpn. J. Appl. Phys*., **33**, 4389 (1994).
8. M. H. Licheng, R. B. Timmons, W. W. Lee, Y. Chen and Z. Hu, *J. Appl. Phys.*, **84**(1), 439 (1998).
9. E. Bapin and Rudolf von Rohr Ph., *Surf. Coat. Technol*., **142-144**, 649 (2001).
10. D.-J. Kim and K.-S. Kim, *AIChE J*., **48**(11), 2499 (2002).
11. D.-J. Kim, K.-S. Kim and Q.-Q. Zhao, *J. Nanoparticle Res*., **5**, 221 (2003).
12. K.-S. Kim, D.-J. Kim, J. H. Yoon, J. Y. Park, Y. Watanabe and M. Shiratani, *J. Colloid Interface Sci*., **257**, 195 (2003).
13. F. Gelbard, Y. Tambour and J. H. Seinfeld, *J. Colloid Interface Sci*., **76**(2), 541 (1980).
14. J. D. Landgrebe and S. E. Pratsinis, *J. Colloid Interface Sci*., **139**(1), 63 (1990).
15. C.-Y. Wu and P. Biswas, *Aerosol. Sci. Technol*., **29**, 359 (1998).
16. J. J. Wu and R. C. Flagan, *J. Colloid Interface Sci*., **123**(2), 339 (1988).
17. T. Matsoukas and M. Russell, *J. Appl. Phys.*, **77**(9), 4285 (1995).
18. A. Anders, *Surf. Coat. Technol*., **183**, 301 (2004).
19. S. Ashida and M. A. Lieberman, *Jpn. J. Appl. Phys.*, **36**, 854 (1997).
20. M. J. Kushner, *J. Appl. Phys.*, **63**, 2532 (1988).
21. B. Ramamurthi and D. J. Economou, *J. Vac. Sci. Technol. A*, **20**(2), 467 (2002).